VLT Observations of the Peculiar Globular Cluster NGC 6712, III: The Evolved Stellar Population [1]

Barbara Paltrinieri[2], Francesco R. Ferraro[3], Francesco Paresce[4], Guido De Marchi[4,5,6]

Received _____; accepted _____

Astronomical Journal in Press

[1]Based on data taken at the VLT, European Southern Observatory, Chile, as part of the ESO observing programme and 63.L-0423(A).

[2]Istituto di Astronomia — Universitá La Sapienza, Via G.M. Lancisi 29, I–00161 Roma, Italy; barbara@coma.mporzio.astro.it

[3]Osservatorio Astronomico di Bologna, via Ranzani 1, I–40126 Bologna, Italy; ferraro@bo.astro.it

[4]European Southern Observatory, Karl Schwarzschild Strasse 2, D–85748 Garching bei München, Germany; fparesce@eso.org

[5]Space Telescope Science Institute, 3700 San Martin Drive, Baltimore, MD 21218, USA; demarchi@stsci.edu

[6]Affiliated to the Astrophysics Division, Space Science Department of ESA

ABSTRACT

We present extensive UBVR photometry of the Galactic globular cluster (GGC) NGC 6712 obtained with the ESO Very Large Telescope (VLT) which reach down to two magnitudes below the main sequence turn-off and allows us for the first time to determine the age of this cluster. By using the apparent luminosity of the zero age horizontal branch (ZAHB), $V_{ZAHB} = 16.32 \pm 0.05$ and the stellar main sequence (MS) turn–off (TO) magnitude $V_{TO} = 19.82 \pm 0.10$, we obtain $\Delta V_{TO}^{HB} = 3.5 \pm 0.1$ (a value fully compatible with that derived for other clusters) which suggests that, at an age of ~ 12 Gyr, NGC 6712 is coeval with other GGC of similar metallicity.

We derive interstellar reddening by comparing the position and morphology of the red giant branch (RGB) with a wide variety of reference clusters and find $E(B-V) = 0.33 \pm 0.05$, a value significantly lower than had been determined previously. Assuming this value for the reddening, we determine a true distance modulus of $(m-M)_0 = 14.55$, corresponding to a distance of ~ 8 kpc.

We find a population of 108 candidate blue straggler stars (BSS), surprisingly large when compared with the typical BSS content of other low concentration clusters. Moreover, we detect a very bright blue star in the core of NGC 6712 that might be a post-AGB star. These results, combined with those already presented in two companion papers, strongly support the hypothesis that NGC 6712 was, at some early epoch of its history, much more massive and concentrated. The continued interaction with the bulge and the disk of the Galaxy has driven it toward dissolution, and what we now observe is nothing but the *remnant* core of a cluster that once was probably one of the most massive in the Galaxy.

Subject headings: globular clusters: individual (NGC 6712); stars: Population II — stars: evolution –

1. Introduction

NGC 6712 is a low-concentration ($c = 0.9$, $Log\rho_0 \sim 3$;, Djorgovski & Meylan 1993), intermediate-high metallicity ($[Fe/H] = -1.01$ Zinn 1985) globular cluster, which has, without doubt, some peculiar characteristics. First, it is the lowest density GGC containing a low mass X-ray binary (LMXB - namely $1RXSJ185304.8-084217$; Voges et al. 1999). LMXB are thought to form via tidal capture in high density clusters, thus the presence of such an object in the core of a loose cluster is somewhat surprising. Second, its orbit, as computed by Dauphole et al. (1996), suggests that it is experiencing a severe interaction with the Galaxy due its numerous passages through the disk and bulge.

Within this intriguing scenario, we have undertaken a detailed study of the global stellar population in NGC 6712, using the ESO *Very Large Telescope*. This is the third paper in a series dedicated to this cluster.

Ferraro et al.2000a (hereafter *Paper I*), besides confirming the optical counterpart to the LMXB, discovered the presence of an additional interacting binary candidate (showing strong UV and $H\alpha$ excess) in the core of NGC 6712, located a few arcsec from the LMXB.

Deep V- and R-band observations of the lower MS, presented by Andreuzzi et al. 2001 (hereafter *Paper II*) confirmed the previous findings by De Marchi et al. (1999) that the mass function of this cluster has been severely depleted of lower mass stars, probably stripped away by the tidal force of the Galaxy.

These results add further support to the scenario that NGC 6712 is only a pale remnant of a once much more massive cluster. Takahashi & Portegies Zwart (2000), using extensive N-body simulations, have recently shown that the inverted mass function observed by De Marchi et al. (1999) is a clear signature of significant mass evaporation since it only appears in clusters which have lost most (up to $\sim 99\%$) of their initial mass. If this scenario is confirmed, with a current mass of $\sim 10^5 M_\odot$ (Pryor & Meylan 1993) NGC 6712 might have been one of the most massive clusters ever formed in the Galaxy with $M_{inital} \sim 10^7 M_\odot$.

In this paper, we make use of a large data-set obtained with the VLT in order to present and discuss the overall morphology and the main characteristics of the CMD for stars brighter than the MS TO, looking for any additional signature of the stormy past of this cluster.

The plan of the paper is as follows. We present the observations and data analysis Section 2 while the overall properties of the resulting colour–magnitude diagramme (CMD) are described in Section 3. Sections 4, 5, 6, 7 are devoted each to the description of one of the evolutionary sequences (horizontal branch - HB, RGB, blue straggler stars - BSS, and blue objects, respectively). A discussion of the cluster age and distance is given in Section 8. Section 9 summarises the main results of this work.

2. Observations and data reductions

2.1. Observations

A large set of frames covering the central region of NGC 6712 was obtained in service mode during June 1999 at the *ANTU* Very Large Telescope (VLT-UT1) at ESO on Cerro Paranal (Chile) using the FORS1 camera equipped with a 2048×2048 pixel^2 CCD array). The data were obtained using two different levels of resolution: *(i)* high resolution (HR), with a plate-scale of $0\farcs1/pixel$ and a field of view of $3\farcm4 \times 3\farcm4$; and *(ii)* standard resolution (SR) with a plate-scale of $0\farcs2/pixel$ and a field of view of $6\farcm8 \times 6\farcm8$. HR frames were roughly centered on the cluster centre, while the four partially overlapping SR fields (one for each quadrant, Q1, Q2, Q3, Q4, respectively) were roughly centered at $3\farcm5$ for the cluster centre(see Figure 1). This configuration allowed us to observe the innermost regions of the cluster with the most appropriate resolution and to cover a large area ($\sim 13\farcm \times 13\farcm$) around the cluster.

The data consist of five 10 s B-, V-, R-band exposures, five 120 s U-band exposures for each HR and SR field. An additional 700 s $H\alpha$ exposure was obtained only in the HR field.

2.2. Magnitudes, colour and positions

All the reductions were carried out using ROMAFOT (Buonanno et al. 1983, Buonanno & Iannicola 1986), a package specifically developed to perform accurate photometry in crowded fields. Specific subroutines of this package have been used to detect stars in each frame, in particular independent searches have been performed in the best blue (U, B) and in the best red (V, R) images, in order to properly optimize the search for blue and red objects. The *blue* and the *red* masks built in this way and containing the position of the stars have been then adapted to each *colour-group* image of the same field (the red mask to all the V- and R-band images and the blue mask for the U and B frames) and the standard PSF-fitting procedure performed. The output instrumental magnitudes in the same band were then averaged by properly weighing the photometric quality of individual frames to yield the adopted *u,b,v,r* mean instrumental magnitudes. The data-sets were then matched together and a final catalogue with stellar coordinates and the average instrumental magnitude in each filter has been compiled for all the objects identified in each of the FORS1 fields.

Stars in overlapping areas (see Figure 1) were used to transform the X and Y coordinates of each field to a common coordinate system. Multiple measurements of the objects common to adjacent SR fields were averaged, while for objects common to HR and a SR field, the HR magnitudes were taken owing to the higher resolution and quality of these images. The result of this procedure is a homogeneous set of instrumental magnitudes, colours and positions for all the stars in our frames.

2.3. Calibration

The final instrumental magnitudes were then transformed into the standard Johnson photometric system by using ten photometric standard stars in selected areas PG1528, PG2213, PG2331 (Landolt 1992). Standard aperture photometry was performed on these stars. The calibration curves linking the instrumental aperture photometry to the Johnson magnitudes are

plotted in Figure 2. A subset of the brightest, unsaturated and most isolated stars was used to link the *instrumental* magnitudes obtained with PSF fitting to those derived with aperture photometry.

$H\alpha$ magnitudes were treated and calibrated as R-band images, except for an offset of ~ 4 mag that was applied so as to account for the lower filter efficiency.

The calibrated data can be compared with the photographic V- and B-band data of Cudworth (1988, hereafter C88): the residuals in magnitude computed using a sample of ~ 100 stars in common with C88 turn out to be very small in both the B and V filters ($V - V_{C88} = 0.00$ and $B - B_{C88} = -0.03$) showing an excellent agreement between the photometric zero-points used here and those of C88.

2.4. Photometric errors

Since we have 5 repeated exposures through each filter, the internal accuracy of our photometry has been estimated from the rms frame-to-frame scatter of the instrumental magnitudes. We computed this quantity for each individual star according to the formula given in Ferraro et al. (1991). The rms values obtained for the U, B, V and R frames are plotted in Figure 3 as a function of the mean final calibrated magnitude adopted for each star measured in the HR field. The mean photometric errors are very small ($\sigma < 0.05$) over the whole magnitude range covered by our observations in all filters.

3. Colour-Magnitude Diagrammes: overall structure

As result of the procedure described in the previous section, a catalogue with magnitudes, colour and positions for a sample of 30,000 stars has been obtained in the region covered by our

observations[7] (see Figure 1). Figure 4 shows the CMD corresponding to stars in regions located at different distances from the cluster centre. In particular, in *panel (a)* all the stars lying in the HR field are plotted while the other three panels (*(b),(c)* and *(d)*, respectively) show the stars located in annuli at increasing distances from the cluster centre. Here the centre of the cluster has been assumed to be the one defined in *Paper I*.

The inspection of the CMD presented in Figure 4 shows that field contamination is particularly severe around NGC 6712. This was to be expected, since the cluster is located behind the Scutum stellar cloud which is one of the highest surface brightness regions in the Milky Way.

The overall characteristics of the CMD in Figure 4 can be summarised as follows:

- (1) The population sampled by the HR field is dominated by cluster stars: all sequences in the CMD, namely the RGB, HB, sub-giant branch (SGB), TO region, BSS sequence, are well defined and populated. The field component, however, is also visible (note the field MS crossing the diagram from $B-V \sim 0.4, V \sim 14.$ down to $B-V \sim 1.2, V \sim 20.5$);

- (2) as expected, at increasing distance from the cluster centre, the field contribution rapidly increases with respect to the cluster population;

- (3) although in the region $150'' < r < 360''$ the field population dominates the overall morphology of the CMD, some features of the cluster population are still visible, such as a few blue HB stars at $18 < V < 17$ and $(B-V) < 0.5$ (see Figure 4*b* and 4*c*).

- (4) blue HB stars are not visible in the CMD at distances $r > 360''$ (see Figure 4 *d*).

[7]The electronic version of the table listing magnitudes and positions for the entire sample is available upon request from the second author (e-mail: ferraro@bo.astro.it)

3.1. Field decontamination

Some features in Figure 4 show that the cluster population is still present in the region $150'' < r < 360''$, even if evolutionary sequences are not clearly defined in the CMD. On the other hand the absence of blue HB stars for $r > 360''$ suggests that the cluster population becomes negligible beyond this distance.

This indication is fully confirmed by the investigation of MS stars presented in *Paper II*, where we compared the MS cluster population at different distances from the cluster centre with that obtained in a reference field taken at much larger distance ($\sim 42'$). From this comparison we concluded that the stellar population at $r > 5'$ from the cluster centre is fully consistent with that observed in the reference field, i.e. it is made almost exclusively of field stars. In Figure 5 we present the projected density distribution (*filled circles*) for the evolved population of the cluster. All stars with $V < 20$ plotted in Figure 4 have been counted. The stellar density has been scaled to match the density profile of MS stars with $19.5 < R < 20.5$ (corresponding to $\sim 0.75 M_{\odot}$) and $r > 2'$ (plotted as *large open squares* in Figure 5 – see also Figure 8 in *Paper II*). The figure clearly shows a plateau in the stellar density for $r > 4.2'$, which is fully consistent with the density of $0.75 M_{\odot}$-mass star measured in the control field at $42'$ from the cluster centre (indicated as the *dotted horizontal line* in Figure 5). This confirms that the cluster population becomes indeed negligible for $r > 5'$.

On the basis of these considerations, we conservatively assumed that the sample at $r > 360''$ can be regarded as field population (see Figure 4(d)) and used it in order to decontaminate the CMD.To be sure, exact discrimination between cluster and field members is not possible on the basis of the CMD comparison alone. However, in order to study the global characteristics of the stellar population of NGC 6712, we adopted a statistical approach, following the method described by Mighell et al. (1996) and successfully used by others as well (see for example Bellazzini, Ferraro & Buonanno, 1999, Testa et al. 1999). In short, for each star in the *contaminated* CMD, the probability of membership is computed by comparing the number of stars lying within a cell (of assigned size) in the *contaminated* CMD and in the *field* CMD.

The decontamination procedure has been applied to each of the CMD plotted in Figure 4 *a, b, c.* Only in the case of the HR field, however, does the procedure yield acceptable results. Figure 6 shows the statistically decontaminated CMD of the HR field. Here the result is quite good as the statistical decontamination successfully removes most of the field stars from the HR CMD and the cluster sequences appear well defined. For this reason, we conservatively decided to limit the analysis of the stellar population of NGC 6712 to this region.

3.2. Cluster population: ridge lines

Figure 5 shows that all the sequences in the CMD are well defined and populated. Particularly noteworthy is the large population of BSS (see Section 6) which has not been affected by the field decontamination procedure as the field MS appears to be significantly redder than the BSS sequence (see Figure 4*a* and 4*d*), mostly because of the higher metallicity of the field population.

The mean ridge lines of the main branches (RGB, SGB) in the CMD plotted in Figure 6 were determined following an iterative process. A first rough selection of the candidate RGB stars was performed by eye, removing the HB and part of the AGB stars. Then, the sample was divided into 0.4 V-mag wide bins and the median colour and magnitude computed in each bin. Stars more distant than 2σ from the median point were rejected and the median and σ recomputed until no more outliers were found, The median points were then interpolated through a spline over an interval of typically 3 magnitudes. The resulting ridge line for the RGB-SGB and TO-MS region is listed in Table 1.

4. The HB morphology and the ZAHB level

Figure 7 plots HB stars from the decontaminated sample of Figure 6. The bulk of the HB stars populates the red side of the instability strip, as expected since NGC 6712 is a cluster of intermediate-high metallicity ($[Fe/H]_{Z85} = -1.01$).

Our CCD photometry does not have the proper time-coverage to search for variability, for this reason we identified the RR-Lyrae variables lying in the FORS1-HR field of view from previous studies. The 7 known RR Lyrae variables (namely V1, V5, V6, V12, V18, V19, V20) identified in our field are plotted as large filled triangles in Figure 7. Their position in the CMD clearly shows that we observed these variables at random phases of their pulsation cycle. Since our observations were not homogeneously spread over the pulsation period, we are unable to derive meaningful average magnitudes and colours for these objects.

In order to more quantitatively describe the morphology of the HB, we computed the parameter $HBM = (B - R)/(B + V + R)$ (Lee et al. 1990, but see Fusi Pecci et al. 1992, Buonanno et al. 1997), where B and R are the number of stars bluer and redder than the RR Lyrae gap, respectively, and V is the number of RR Lyrae variables. Using our sample, this parameter takes on the value $HBM = (23 - 127)/(23 + 7 + 127) = -0.66 \pm 0.12$, a figure typical of clusters of intermediate-high metallicity which confirms that the HB morphology of NGC 6712 closely resembles that of NGC 6171 (Ferraro et al. 1991), a cluster with similar metallicity.

To provide a characterisation of the extreme blue HB population with respect to the red one, we also computed Buonanno's (1993) index $P_{HB} = (B2 - R)/(B + V + R)$, where $B2$ is the number of the blue HB stars bluer than $(B - V)_0 = -0.02$. This parameter is, of course, reddening-dependent: assuming $E(B - V) = 0.33$, as explained in Section 5.2,we obtain $P_{HB} = -0.78 \pm 0.14$.

Ferraro et al. (1999a, hereafter F99) presented a new procedure for the determination of the level of the ZAHB in the observed (V,B-V)-CMD. This procedure uses synthetic HB models to reproduce the observed HB morphology. Once a proper agreement between the observed and the synthetic HB has been obtained, the value of V_{ZAHB} can be derived from the model which has been used to construct the synthetic HB.

F99 derived $V_{ZAHB} = 16.32 \pm 0.05$ for NGC 6712 adopting the C88 photometry. As shown in Section 2.3, the C88 photometry nicely agrees with that presented in this paper. Thus, in the following, we adopt this value for the ZAHB level. The ZAHB is shown as a solid line in Figure 6;

as expected, it is consistent with the lower boundary of the magnitude distribution of the red HB clump.

5. The RGB: metallicity and reddening

Once properly calibrated, the shape and position of the RGB in the CMD can be used to derive photometric estimates of the cluster metallicity.

5.1. Metallicity scales

The most widely used metallicity scale for GGC is that proposed by Zinn and collaborators in the 1980s (Zinn & West 1984, Zinn 1985) and essentially based on integrated light indexes and low resolution spectra. There is now a growing body of reasons (see Carretta & Gratton 1997 - herafter CG97 and Rutledge et al. 1997) suggesting a revision of the *classical* Zinn scale, according to the results of the latest high-resolution spectral data which have the advantage of measuring directly Iron absorption lines. In the following, we adopt the CG97 metallicity scale ($[Fe/H]_{CG97}$).

Moreover, there is much observational evidence that α-elements (such as Si and Ca) are often enhanced with respect to Iron for Population II stars and thus the knowledge of the Iron abundance alone in not sufficient to correctly evaluate the *global* metal content in each cluster. For this reason, the *global* metal index ($[M/H]$) (including also the α-element enhancement) has been defined (see Salaris, Chieffi & Straniero, 1993). For a more detailed discussion of this topic, we refer the reader to F99 and Ferraro et al. 2000b, and the references therein.

Here, we just note that NGC 6712 turns out to have, according to Table 2 in F99, the following estimated metallicity in different scales: $[Fe/H]_{Z85} = -1.01$, $[Fe/H]_{CG97} = -0.88$, and $[M/H] = -0.71$.

5.2. RGB parameters: metallicity and reddening

A complete set of RGB parameters and metallicity indicators in the classical $(V, B-V)$ and in the IR plane has been recently presented by F99 and Ferraro et al. (2000b), respectively. These papers also reported on an independent calibration of RGB-parameters in terms of the cluster metallicity (both in the CG97 and *global* scales). In particular, F99 presented a system of equations (see Table 4 in F99) which can be used to simultaneously derive an estimate of metal abundance (in terms of $[Fe/H]_{CG97}$ and $[M/H]$) and reddening from the morphology and location of the RGB in the $(V, B-V)$ CMD. This system of equations is the equivalent to the so-called SRM method defined by Sarajedini (1994) in the $(V, V-I)$ plane.

For NGC 6712 we used the mean ridge line listed in Table 1 to measure three RGB-parameters: $(B-V)_g$, defined as the observed RGB colour at the HB level; the two RGB slopes $S_{2.0}$ and $S_{2.5}$ defined as the slope of the line connecting the intersection of the RGB and HB with the points along the RGB located, respectively, 2.0 and 2.5 mag brighter than the HB. Assuming the ZAHB level obtained in Section 4 and the mean ridge line listed in Table 1, we obtained a first set of RGB parameters, namely $(B-V)_g = 1.26$, $S_{2.0} = 4.69$ and $S_{2.5} = 4.20$ (see F99 for the definition of these parameters). With these values as *"input"*, the method soon achieved convergence on the following values: $E(B-V) = 0.33 \pm 0.05$, $[Fe/H]_{CG97} = -0.80 \pm 0.20$ and $[M/H] = -0.62 \pm 0.20$. The errors associated with the measurements are conservative estimates of the global uncertanties, formal errors being much smaller than those assumed.

The photometric estimate of the cluster metallicity derived with the technique above fully agrees with previous estimates and confirms that NGC 6712 is an intermediate-high metallicity cluster.

On the other hand, the value of the reddening obtained with this procedure appears significantly lower than that listed in the literature: $E(B-V) = 0.48$, Webbink (1986) and $E(B-V) = 0.46$, Harris (1996). Past reddening determinations for this cluster, however, are quite uncertain: 0.48 (Sandage & Smith, 1966), 0.38 (Kron & Guetter, 1976), 0.40 (Alcaino, 1977), 0.33

(Martins & Harvel 1981), 0.42 (Cudworth 1988). Moreover, Janulis & Smriglio (1992) confirmed the existence of differential reddening in the region of NGC 6712.

6. Blue Stragglers

BSS were first observed in the 1950's in the outer region of the GGC M3 (Sandage 1953), while the first sample of BSS in the cores of dense GGC were discovered with HST (Paresce et al. , 1991) in 47 Tuc. Since then, systematic searches for these objects in GGC cores have been performed from the ground and from space. The main result of this extensive search is that they have been found in all the GGC properly observed, thus suggesting that BSS are a normal component of the GGC population (see the catalogue by Sarajedini 1993, and Ferraro, Bellazzini & Fusi Pecci 1995).

BSS are thought to form via two main mechanisms: (1) the merger of two stars in a primordial binary system and (2) stellar collisions (Bailyn 1995, Bailyn & Pinsonneault 1995). Many authors (Bailyn 1992, Fusi Pecci et al. 1992, Ferraro, Bellazzini & Fusi Pecci 1995) suggested that BSS in loose clusters might be produced from the coalescence of primordial binaries, whereas in high density clusters BSS might arise from stellar collisions (depending on the survival-destruction rate of primordial binaries). In particular, collisional BSS can be used as a diagnostic of the dynamical evolution of GGC (see, for example, the exceptionally large population of BSS recently found in M80 by Ferraro et al. 1999b).

From the analysis of the CMD plotted in Figure 4 and Figure 6, one sees that NGC 6712 has a quite large population of BSS. As already said, this population is not affected by field contamination, since the BSS sequence is significantly bluer than the Field MS.

On the basis of their location in the $(V, B-V)$ CMD we identified a sample of 108 BSS. The identification numbers, the V,B,R and U magnitudes and the X and Y coodinates (in pixels [1 px= 0".1] with respect to the adopted cluster center) for the candidate BSS are listed in Table 2. Figure 8 shows zoomed CMDs where the BSS candidates are plotted as large filled circles. As

can be seen, all the candidates selected in the $(V, B-V)$ CMD lie also in the BSS region in the $(U, U-V)$ CMD. Moreover, this latter CMD suggests that a few additional objects might be considered BSS candidates. We conservatively decided, however, to limit our analysis to those stars which are BSS candidates in both CMDs. In particular, we intended to avoid regions of the CMD which can be populated by *artificial* stars resulting from blending effects (see Ferraro et al. 1991, 1992).

It is worth noticing that five objects slightly redder and brighter that the BSS sequence (plotted as stars in Figure 8) seem to delineate a track for post-BSS evolution (E-BSS evolved BSS). According to their position in the CMD, they could be BSS which have left the MS to evolve toward the RGB (BSS in SGB phase). Candidate BSS in such an evolutionary phase have been observed in other clusters (see for example the CMD of NGC5053 by Nemec & Cohen 1989 or the CMD of the external region of M3, Buonanno et al. 1994). We did not, however, include these stars in our sample as they lie in a region of the CMD where field contamination starts to be severe. Since we performed only a statistical decontamination of the observed sample, cluster membership of stars plotted in Figure 6 cannot be guaranteed, expecially in highly contaminated regions of the CMD. The selected E-BSS candidate are, nevertheless, worth further investigation in order to better assess their membership and true nature and for this reason they are also listed in Table 2.

Even with the conservative selection criterion adopted above, the number of BSS found in the central regions of NGC 6712 is surprisingly large. Although in absolute terms, NGC 6712 has much fewer BSS than M80 (Ferraro et al. 1999b), it shows a population comparable with that of NGC 6388 and NGC2808 (see Sosin et al. 1998) which are much more massive (a factor ~ 16) and concentrated (a factor $\sim 100-500$) than NGC 6712.

In order to quantitatively compare the BSS population across GGC, its fraction with respect to the total has to be taken into account. In doing so, Ferraro et al. (1997, 1999b) defined the specific fraction of BSS $F_{HB}^{BSS} = N_{BSS}/N_{HB}$ as the number of BSS normalised to the number of HB stars observed in the same cluster region. In NGC 6712 the specific frequency calculated

in this was is ~ 0.69 similar to that obtained in M3 (Ferraro et al. 1999b) which is again more massive ($M_V = -8.75$) and concentrated ($c = 2.0$) than NGC 6712.

If one limits the comparison to clusters with similar structure (for example with comparable concentration $c \sim 1$ and integrated magnitude), this population appears indeed large. Note that NGC5897 ($M_V = -7.27$ and $c = 0.95$), for example, has only 34 BSS (Ferraro, Fusi Pecci & Buonanno 1992) and $F_{HB}^{BSS} = 0.5$.

Generally, BSS are more centrally concentrated with respect to the other stars in the cluster, although there are notable exceptions to this general rule, such as M 3 (Ferraro et al. 1993, 1997) and M 13 (Paltrinieri et al. 1998). In NGC 6712 we compared the radial distribution of BSS with respect to RGB and SGB objects (in the range $17.5 < V < 20$). The cumulative radial distributions are plotted, as a function of the projected distance (r) from the cluster centre, in Figure 9, where one sees that BSS (solid line) are more centrally concentrated than the RGB+SGB sample (dashed line). The Kolmogorov-Smirnov test shows that the probability of drawing the two populations from the same distribution is only 0.1%. The two distribution are, thus, different at a high level of significance ($> 3\sigma$).

7. Blue Objects

7.1. A post-AGB bright object, or two?

Figure 6 shows that a few blue objects are present in the very central regions of NGC 6712. The three faint blue objects ($V > 19$ and $B - V < 0.5$), namely star #10261, #9774 and #8916, in our catalogue, have been discussed in *Paper I*. In particular, star #9774 is star S of Anderson et al. (1993) and, on the basis of its position, is the best candidate to the optical counterpart to the luminous X-ray source detected in this cluster. Star #10261 is a relatively bright UV star, located a few arcsec away from the X-ray source, and it is the only object in the HR-field showing a significant $H\alpha$ emission (see next Section). For these reasons, in *Paper I* we suggested it is an additional promising interacting binary candidate.

From the analysis of Figure 6, it is also evident that the bluest object in the CMD is a bright star (namely #9620) roughly located at the HB level, $V = 16.67$ but significantly bluer ($B - V = 0.03$) than the bluest HB stars ($B - V \sim 0.3$)

Figure 10 shows the $(U, U - B)$ CMD of all the stars plotted in Figure 6, and star #9620 still shows as the most UV-bright object in the field. The three faint UV stars discussed in *Paper I* are plotted as open triangles.

The position of the UV-bright star in the CMD closely resembles that of the UV-bright post-AGB star found in M3 (vZ1128, see Buonanno et al. 1994). Such objects are indeed very rare in GGC: only a few post-AGB stars have been found in GGC due to their short evolutionary lifetime of $\sim 10^5$ yr (only 0.5 Post-AGB stars are expected to be found in a typical $\sim 10^5 L_\odot$ cluster).

To assess whether the position of star #9620 is compatible with that of a post-AGB star, we performed a qualitative comparison with theoretical models. A $t \sim 12.5$ Gyr (see Section 8.2) isochrone with appropriate metallicity ($Z = 0.004$) from Bertelli et al. 1994 has been over-plotted in the CMD of Figure 10, after having been shifted to fit the main loci, so as to mark the location in this diagramme of the post-AGB track and the subsequent cooling sequence. The location of star #9620 in the CMD nicely agrees with that predicted by the models.

Note that star #9620 is located only $\sim 19''$ away from the cluster centre. Although, in principle, we cannot exclude that this object is a field star, it is worth noting that no similar UV-bright objects have been found in the sample that we assumed as FIELD (see Figure 4d). Moreover, another similar UV-bright object (lying in the same region of the CMD) has been found in the field labelled as SR-Q1 in Figure 1, at $4.4'$ from the cluster centre (see Figure 4c). These objects deserve a more detailed spectroscopic analysis, as proving that both are cluster members would add further support to the scenario that NGC 6712 was much more massive in the past.

7.2. The $(H\alpha, H\alpha - R)$ CMD

Some stars in GGC are expected to show $H\alpha$-emission: a few bright red giants (see Cacciari & Freeman 1983) or rare objects possibly connected to planetary nebulae (see Jacoby et al. 1997) or some exotic objects connected to interacting binaries (as cataclysmic variable and LMXB; see Cool et al. 1995). According to Cool et al. 1995, the $(H\alpha, H\alpha - R)$ CMD can efficiently serve the purpose of revealing $H\alpha$-excess objects. Indeed, in this diagramme stars with $H\alpha$ in absorption will have $(H\alpha - R) > 0$ while stars with $H\alpha$ in emission will feature $(H\alpha - R) < 0$. Typical cool giants and SGB stars in a cluster will have a weak $H\alpha$ absorption line ($EW(H\alpha) = 1A$) and, for this reason, they will have $(H\alpha - R) \sim 0$.

Figure 11 shows the $(H\alpha, H\alpha - R)$ CMD for stars in the HR field. The brightest RGB stars are saturated in the long $H\alpha$ exposure, so they are not plotted in that figure. As expected, the bulk of the cluster population, constitued as it is by relatively cool stars, defines a sequence lying in the CMD at $H\alpha - R \sim 0$. The $H\alpha$-excess star discussed in *Paper I* is marked by its identification number in our catalogue. Interestingly enough, on the right of the main sequence there are a few stars which seem to define a secondary sequence at $(H\alpha - R) \sim 0.15$ almost parallel to the main one. According to their position in this diagramme, they should have $H\alpha$ in absorption. These stars are the hottest HB stars and BSS. In particular, blue HB stars (with $(B - V) < 0.5$ see Figure 6) which are plotted as large filled circles define a very narrow sequence, well defined and well separated from the main one. The bright UV-object (star #9620) discussed in the previous section is plotted in Figure 11 as an open square. According to its position it turns out to have an $H\alpha$ absorption line of intensity intermediate between that of giants and blue HB stars.

Figure 11 shows that the $(H\alpha, H\alpha - R)$ CMD can be used as an independent method to select blue HB stars, and can provide a direct measure of the strength of the $H\alpha$ absorption line in these stars (see Cool et al. 1995).

8. Turn-Off point and age

8.1. Comparison with NGC 6171: the relative age of NGC 6712

An accurate determination of relative ages of GGC provides fundamental clues to the formation time-scale of the Galactic halo (see Buonanno, Corsi & Fusi Pecci 1989, Vandenberg, Stetson & Bolte 1996, Rosenberg et al. 1999 -hereafter R99- and reference therein).

Since the SGB-TO region in the CMD plotted in Figure 6 is very well defined and populated, we can use it to locate the MS-TO, which is, as well known, a good age indicator.

As mentioned above, the whole CMD of NGC 6712 closely resembles that of NGC 6171, a cluster with similar metallicity. In Figure 12 the mean ridge lines of NGC 6171 (solid lines) from Ferraro et al. 1991, have been shifted (by $\Delta V = 0.65$ and $\Delta(B-V) = 0.0$) to match the CMD of NGC 6712. The ZAHB level for NGC 6171 has been assumed to be $V_{ZAHB} = 15.70 \pm 0.10$ according to Table 2 of F99). Figure 12 shows that the mean loci of NGC 6121 agree quite nicely with the CMD of NGC 6712. Small residual differences in colour between the mean ridge line and the CMD in the extreme red region and at the TO region are probably due to small residual uncertainties in the colour equation affecting the relatively old photometry of NGC 6171.

Note that the lack of any colour shift corresponds exactly to what is expected for these two clusters since they have formally the same reddening (see Ferraro et al. 1991 for NGC 6171).

To obtain a quantitative estimate of the relative age of the two clusters we used the so-called *vertical method*: this is the most widely used relative-age indicator, based on the TO luminosity with respect to the HB level (Buonanno, Corsi & Fusi Pecci 1989).

From Table 1, the TO level in NGC 6712 is located at $V_{TO} = 19.82 \pm 0.10$. Using this value and the V_{ZAHB} computed in Section 4, we derived $\Delta V_{TO}^{HB} = 3.50 \pm 0.15$ mag. For NGC 6171, assuming $V_{TO}^{NGC\,6171} = 19.20 \pm 0.10$ (Ferraro et al. 1991) and $V_{ZAHB}^{NGC\,6171} = 15.70 \pm 0.10$ (from F99), we found $\Delta V_{TO}^{HB} = 3.50 \pm 0.15$ mag.

From this comparison, we can conclude that NGC 6712 is nearly coeval with NGC 6171. On the other hand, NGC 6171 has been found (R99) to be coeval with other clusters belonging to the

same metallicity class (NGC288, NGC 6218, NGC 6362, NGC 6723). Thus, we can safely conclude that NGC 6712 does not show any significant difference in age with respect to the bulk of the intermediate metal-rich population of GGC.

8.2. Cluster distance and absolute age

The evaluation of absolute ages requires the knowledge (or the implicit assumption) of the distance modulus for the cluster. Different loci in the CMD have been assumed in the past as standard candles (HB - see F99, MS - see Gratton et al. 1997, WD - see Renzini et al. 1996) to determine cluster distances. F99 used the HB and, in particular, the ZAHB as a reference candle and derived a new homogeneous distance scale for a sample of 64 GGC. Here we use the same procedure to derive the distance to NGC 6712.

The Straniero Chieffi & Limongi (1997) theoretical HB models were used to derive the absolute magnitude of the ZAHB as a function of the metallicity (see eq. 4 in F99). From this relation and assuming $[Fe/H]_{CG97} = -0.8$ (section 5.2), we get $M_V^{ZAHB} = 0.75$. Assuming $V_{ZAHB} = 16.32$ (see Section 4), we obtain an apparent distance modulus $(m-M)_V = 15.57$ and finally (considering $E(B-V) = 0.33$, see Section 5.2) a true modulus of $(m-M)_0 = 14.55$, which corresponds to a distance of ~ 8.1 Kpc.

This value turns out to be significantly larger than that obtained by C88 (6.5 Kpc). The origin of such a large discrepancy is due to many differing assumptions between C88 and this paper. First of all, the reddening adopted here ($E(B-V) = 0.33$) is quite different from that used by C88 ($E(B-V) = 0.42$). Second, the assumption of the absolute level of the HB is different: C88 used $M_V^{HB} = 0.85$ and we used $M_V^{HB} = 0.75$ and finally there is a small difference (0.07 mag) in the observed value of the HB level (C88 used $V_{HB} = 16.25$).

In addition, C88 adopted the relation $A_V = 3.2E(B-V)$ instead of the canonical $R_V = 3.1$. This (or even higher) value of R_V can be reasonable for NGC 6712 since it is in a highly contaminated region. Although the different assumption for R_V between us and C88 produces

only a small effect(~ 0.04 mag), the impact of a different R coefficient on the determination of the true distance modulus of NGC 6712 should be kept in mind. At the moment, however, the main source of uncertainty in the distance error budget is the reddening: the assumed error (± 0.05), in fact, produces an uncertainty of ~ 0.15 mag in the distance modulus and an error of $\sim 6\%$ (~ 0.5 Kpc) in the true distance. Taking into account this and the uncertainties on the other parameters concurring to the determination of the distance, we finally conclude that the global uncertainty cannot be less than 10% and assume $d = 8 \pm 1$ Kpc as a final conservative estimate of the distance to NGC 6712.

From the distance modulus obtained above and $V_{TO} = 19.82 \pm 0.10$ (from Table 1), we get $M_V^{TO} = 4.25 \pm 0.2$. With this value and the metallicity estimate ($[Fe/H]_{CG97} = -0.8$) obtained in Section 5.2, we can derive the age for NGC 6712 using theoretical relations linking these observables to the cluster age. In doing so, we used the relations recently obtained by R99 (see their Appendix A), for three sets of theoretical models: SCL97, Cassisi et al. (1998) and VandenBerg et al. (2000) and obtained $t = 12.6$, 12.9 and 11.5 Gyr, for SCL97, Cassisi et al. (1998) and VandenBerg et al. (2000), respectively. Taking into account that the global uncertainty of the method can hardly be better than 15%, we conservatively assume $t = 12 \pm 2$ Gyr as the absolute age of NGC 6712.

9. Summary and Conclusions

In this paper we have presented extensive, high resolution, $UBVR$ photometry of the galactic globular cluster NGC 6712, obtained with the ESO-Very Large Telescope. This data set gives us the opportunity to investigate the evolved stellar population of the cluster, yielding new constraints on its metallicity, age and structural parameters. In particular we find the following results:

- *Metallicity and Reddening:* The location and morphology of the RGB in the (V,B-V)-CMD, compared with a large set of reference clusters, fully confirm that NGC 6712

is an intermediate metal-rich cluster. Using the method described in F99 we get $[M/H] = 0.62 \pm 0.2$, $[Fe/H]_{CG97} = -0.80 \pm 0.2$. The method also yields an estimate of the reddening which turns out to be $E(B-V) = 0.33 \pm 0.05$, a value significantly lower than previously thought.

- *Distance:* Using the theoretical level of the ZAHB (from SCL97) as a reference candle, we derived $(m-M)_V = 15.57$ and a true distance modulus $(m-M)_0 = 14.55$ which corresponds to a distance of about ~ 8 Kpc. This value is significantly higher than that obtained by C88 (who found 6.5 Kpc), mainly because of the new reddening determination.

- *Age:* Coupling the apparent luminosity of the ZAHB, $V_{ZAHB} = 16.32 \pm 0.05$ with $V_{TO} = 19.82 \pm 0.10$, we get $\Delta V_{TO}^{HB} = 3.5 \pm 0.1$, a value fully compatible with that obtained in other clusters. This suggests that NGC 6712 is nearly coeval, at least, with other clusters with similar metallicity. An average absolute age of $t = 12 \pm 2 Gyr$ has been derived from comparison with the theoretical models.

- *BSS:* The cluster reveals a large population of BSS: we selected a sample of 108 BSS from $(V, B-V)$ and $(U, U-V)$ CMD. This number is surprisingly large when compared with the BSS population of clusters with similar mass and central concentration.

- *Post-AGB star:* We discovered the presence of a bright UV-bright object in the core, whose position in the CMD closely matches that of a star evolving in the post-AGB phase. A second objects with similar characteristics has been located further out in the cluster at $\sim 4\farcm4$ from the centre.

The overall scenario emerging when we combine some of the results listed above with those already presented in the two previous papers of this series (*Paper I* and *II*), is quite exciting.

NGC 6712 is experiencing a severe interaction with the disk and the bulge of the Galaxy, as suggested by its orbit (Dauphole et al. 1996). The existence (presented in De Marchi et al. 1999, and confirmed by *Paper II*) of an *inverted* mass function due to a severe depletion of low mass

stars in the MS luminosity function, probably stripped away by the tidal force of the Galaxy, fully supports this scenario.

Takahashi & Portegies Zwart (2000), using N-body simulations, interpreted this rare feature as a clear signature of severe mass loss and suggested that NGC 6712 might be only the remnant "core" of a once much more massive cluster, that has lost most (up to $\sim 99\%$) of its initial mass through the interaction with the Galaxy. Thus the hypothesis that NGC 6712 might have been much more massive (and, possibly, much more concentrated) in the past, gained support from a theoretical point of view.

Now, this scenario finds additional support from a variety of observational facts. The presence of a LMXB and our recent discovery (*Paper I*) of an additional promising interacting binary candidate located a few arcsec away from the optical counterpart to the LMXB, suggest that strong stellar interactions might have occurred at some remote stage of the cluster evolution. Moreover, the large BSS population discovered in this paper adds additional support to the fact that star collisions might have occurred in the past, generating most (or part) of the observed BSS. At that time, NGC 6712 probably was a massive and concentrated cluster and collisional BSS (and other exotic objects such as interacting binaries) formed copiously via dynamical collisions. Then, these stars have migrated towards the centre, because of mass segregation, where we now see them. The continued action of tidal stripping and disk shocking has removed most of the cluster mass, driving it towards dissolution. What we now observe is nothing but the remnant core of a disrupting cluster and its population of peculiar objects, which are otherwise totally unexpected for its actual mass.

If this scenario is further confirmed, our observations would have served the purpose of reconstructing the stormy history of NGC 6712 and possibly, for the very first time, to characterize the effects of the disk shocking on the evolution of stars in a globular cluster.

This research was partially supported by the *Agenzia Spaziale Italiana* (ASI). The financial support of the *Ministero della Università e della Ricerca Scientifica e Tecnologica* (MURST) to

the project *Stellar Dynamics and Stellar Evolution in Globular Clusters* is kindly acknowledged. F. R. F. gratefully acknowledges the hospitality of the *Visitor Program* during his stay at ESO, when most of this work has been carried out. The data presented in this paper were obtained as part of an ESO Service Mode programme.

REFERENCES

Alcaino, G., 1977, PASP, 89, 491

Anderson, S. F., Margon, B., Deutsch, E.,W., Downes, R.A., 1993, AJ, 106, 1049

Andreuzzi, G., et al. , 2001, A&A, in press *(Paper II)*

Bailyn, C.D., 1992, ApJ, 392, 519

Bailyn, C.D., 1995, ARA&A, 33, 133

Bailyn, C.D., Pinsonneault, M.H., 1995, ApJ, 439, 705

Bellazzini, M., Ferraro, F.R., Buonanno, R., 1999, MNRAS, 307, 619

Bertelli, G., Bressan, A., Chiosi, C., Fagotto, F., Nasi, E. 1994, A&AS, 106, 275

Buonanno, R., Buscema, G., Corsi, C.E., Ferraro, I., Iannicola, G. 1983, A&A, 126, 278

Buonanno, R., Corsi, C. E., Fusi Pecci, F. 1989, A&A, 216, 80

Buonanno, R. & Iannicola, G. 1989, PASP, 101, 294

Buonanno, R., 1993, in ASP Conf. Ser. 48, The globular cluster-Galaxy connection, ed. G.H. Smith & J.P. Brodie, (San Francisco: ASP), 131

Buonanno, R., Corsi, C.E., Buzzoni, A., Cacciari, C., Ferraro, F.R., Fusi Pecci, F. 1994, A&A, 290, 69 (PH94)

Buonanno, R., Corsi, C., Bellazzini, M., Ferraro, F. R., Fusi Pecci, F. 1997, AJ, 113, 706

Cacciari, C., Freeman, K. C. 1983, ApJ, 268, 185

Carretta, E., Gratton, R. G. 1997, A&AS, 121, 95

Cassisi, S., Castellani, V., degl'Innocenti, S., Weiss, A. 1998,

A&AS, 129, 267

Cool, A. M., Grindlay, J. E., Cohn, H. N., Lugger, P. M., Slavin, S. D. 1995, ApJ, 439, 695

Cudworth, K.M. 1988, AJ, 96, 105 (C88)

Dauphole, B., Geffert, M., Colin, J., Ducourant, C., Odenkirchen, M., Tucholke, H.-J., 1996, A&A, 313, 119

De Marchi, G., Leibundgut, B., Paresce, F., Pulone, L., 1999, A&A, 343, 9

Djorgovski, S. G. 1988, in The Harlow-Shapley Symposium on Globular Cluster Systems in Galaxies, ed. J. E. Grindlay & A. G. D. Philip (Dordrecht: Kluwer), 333

Djorgovski, S., Meylan, G., 1993, in Structure and Dynamics of Globular Clusters, ed. S. G. Djorgovski & G. Meylan (ASP: San Francisco), 325

Ferraro, F.R., Clementini, G., Fusi Pecci, F., Buonanno, R., 1991, MNRAS, 252, 357

Ferraro, F.R., Fusi Pecci, F., Buonanno, R., 1992, MNRAS, 256, 376

Ferraro, F.R., Clementini, G., Fusi Pecci, F., Sortino, R., Buonanno, R., 1992, MNRAS, 256, 391

Ferraro, F.R., Fusi Pecci, F., Cacciari, C., Corsi, C.E., Buonanno, R., Fahlman, G.G., Richer, H.B. 1993, AJ, 106, 2324

Ferraro, F.R., Bellazzini, M., Fusi Pecci, F., 1995, A&A, 294, 80

Ferraro, F.R., Paltrinieri, B., Fusi Pecci, F.,Cacciari, C., Dorman, B., Rood, R.T., Buonanno, R., Corsi, C.E., Burgarella, D., Laget, M., 1997, A&A, 324, 915

Ferraro, F.R., Messineo, M., Fusi Pecci, F., De Palo, M.A., Straniero, O., Chieffi, A., Limongi, M., 1999a, AJ, 118, 1738 (F99)

Ferraro, F.R., Paltrinieri, B., Rood, R.T., Dorman, B., 1999b, ApJ, 522, 983

Ferraro, F. R., Paltrinieri, B., Paresce, F., De Marchi, G. 2000a, ApJ, 542, L29 *(Paper I)*

Ferraro, F. R.,Montegriffo, P., Origlia, L., Fusi Pecci, F., 2000b, AJ, 119, 1282

Fusi Pecci, F., Ferraro, F.R. , Corsi, C.E., Cacciari, C., Buonanno, R. 1992, AJ, 104, 1831

Gratton, R. G., Fusi Pecci, F., Carretta, E., Clementini, G., Corsi, C. E., Lattanzi, M. 1997, ApJ 491, 749

Harris, W.E., 1996, AJ, 112, 1487

Kron, G.E., Guetter, H.H., 1976, AJ, 81, 817

Jacoby, G. H., Morse, J. A., Fullton, L. K., Kwitter, K. B., Henry, R. B. C. 1997, AJ, 114, 2611

Janulis, R., Smriglio, F., 1992, Baltic Astr., 1, 430

King, I. R. 1966, AJ, 71, 64

Landolt, A.U., 1992, AJ, 104, 340

Lee, Y. W., Demarque, P., Zinn, R. 1990, ApJ, 350, 155

Martins, D.H., Harvel, C.A., 1981, ApJ, 250, 135

Mighell, K. J., Rich, R. M., Shara, M., Fall, S. M. 1996, AJ, 111, 2314

Nemec, J. M., Cohen, J. G. 1989, ApJ, 336, 780

Paresce, F., Meylan, G., Shara, M., Baxter, D., Greenfield, P., et al. , 1991, Nature, 352, 297

Paltrinieri, B., Ferraro, F.R., Fusi Pecci, F., Rood, R.T., Dorman, B., 1998, in Ultraviolet Astrophysics Beyond the IUE Final Archive ed. B. Harris, Noordwijk, The Netherlands, p.565

Pryor, C., Meylan, G., 1993, in Structure and Dynamics of Globular Clusters, ed. S. G. Djorgovski & G. Meylan (ASP: San Francisco), 357

Renzini, A., Bragaglia, A., Ferraro, F. R., Gilmozzi, R., Ortolani, S., Holberg, J. B., Liebert, J., Wesemael, F., Bohlin, R. C. 1996, ApJL, 465, 23

Rosenberg, A., Saviane, I, Piotto, G., Aparicio, A. 1999, AJ, 118, 2306 (R99)

Rutledge, G. A., Hesser, J. E., Stetson, P. B., Mateo, M., Simard, L., Bolte, M., Friel, E. D., Copin, Y. 1997, PASP, 109, 883

Sandage, A. R., 1953, AJ, 58, 61

Sandage, A. R., Smith, A., 1966, ApJ, 144, 866

Salaris, M., Chieffi, A., Straniero, O. 1993, ApJ, 414, 580

Sarajedini, A., 1993 in Blue Straggles, ed. R.A. Saffer, ASP Conf Series, 53, 14

Sarajedini, A. 1994, PASP, 106, 205

Sosin, C., Piotto, G., Djorgovski, S. G., King, I.R., Rich, R. M., Dorman, B., Liebert, J., Renzini, A. 1998, in Advances in Stellar Evolution ed. R.T.Rood & A. Renzini (Cambridge: Cambridge U. Press), 92

Straniero, O., Chieffi, A., Limongi, M. 1997, ApJ, 490, 425

Takahashi, K., Portegies Zwart, S.F., 2000, ApJ, 535, 759

Testa, V., Ferraro, F. R., Chieffi, A., Straniero, O., Limongi, M., Fusi Pecci, F. 1999, AJ, 118, 2839

Trager, S.C., Djorgovski, S.G., King, I.R. 1993 in ASP Conf. Ser. 50, Structure and Dynamics of Globular Clusters, ed. Djorgovski S. G. & Meylan, G., (San Francisco: ASP), 347

Vandenberg, D. A., Stetson, P. B., Bolte, M. 1996, ARA&A 34, 461

Vandenberg, D. A., Swenson, F. J., Rogers, F. J., Iglesias, C. A., Alexander, D. R., 2000, ApJ, 532, 430

Voges, W., et al. 1999, A&A, 349, 389

Webbink, R. F. 1986, Highlights of astronomy. Vol. 7 -Proceeding of the Nineteenth IAU General Assembly, Delhi, India. Dordrecht, D. Reidel Publishing Co., 185

Zinn, R. 1985, ApJ, 293, 424

Zinn, R., West, M. J. 1984, ApJS, 55, 45

Table 1. RGB-SGB Mean ridge line

B-V	V	B-V	V	B-V	V
2.110	13.510	1.214	16.700	0.932	19.370
2.048	13.540	1.195	16.900	0.910	19.420
1.978	13.570	1.176	17.100	0.888	19.460
1.909	13.700	1.155	17.300	0.875	19.490
1.824	13.900	1.138	17.500	0.861	19.530
1.761	14.100	1.127	17.700	0.845	19.580
1.691	14.300	1.115	17.900	0.832	19.650
1.640	14.500	1.103	18.100	0.826	19.730
1.580	14.700	1.096	18.300	0.822	19.820
1.521	14.900	1.085	18.500	0.824	19.900
1.478	15.100	1.079	18.700	0.826	19.990
1.435	15.300	1.061	18.930	0.829	20.090
1.392	15.500	1.048	19.110	0.835	20.200
1.356	15.700	1.023	19.220	0.842	20.300
1.325	15.900	1.008	19.250	0.856	20.460
1.288	16.100	0.995	19.280	0.868	20.580
1.261	16.300	0.973	19.310	0.894	20.810
1.240	16.500	0.953	19.330	0.917	21.020

Table 2. BSS candidates in NGC6712

#	ID	V	B	R	U	X	Y
BSS 1	111	19.45	20.18	18.95	20.46	-400.973	-998.374
BSS 2	144	19.36	20.10	18.85	20.20	804.297	-980.577
BSS 3	262	18.56	19.27	18.08	19.58	728.953	-916.481
BSS 4	540	17.75	18.33	17.35	18.65	792.174	-791.430
BSS 5	670	18.02	18.68	17.57	19.05	-322.614	-743.712
BSS 6	1155	18.66	19.31	18.20	19.56	-196.280	-593.166
BSS 7	1177	18.57	19.24	18.11	19.48	-117.403	-598.961
BSS 8	1242	18.79	19.36	18.39	19.71	-45.187	-580.513
BSS 9	1254	18.51	19.25	17.99	19.32	532.380	-579.290
BSS 10	1456	18.93	19.62	18.47	19.84	20.270	-526.844
BSS 11	1504	18.52	19.11	18.12	19.52	303.193	-523.704
BSS 12	1568	18.36	18.93	17.99	19.24	-398.783	-481.762
BSS 13	1571	19.23	19.96	18.76	20.15	-426.108	-486.179
BSS 14	1742	18.76	19.43	18.28	19.65	-76.106	-473.851
BSS 15	1850	18.58	19.35	18.06	19.63	-638.202	-449.283
BSS 16	1903	19.12	19.77	18.64	19.95	112.571	-438.082
BSS 17	1906	18.77	19.54	18.22	19.76	120.261	-427.270
BSS 18	1920	19.48	20.14	19.03	20.44	-190.172	-436.096
BSS 19	1930	19.00	19.66	18.54	19.92	-888.934	-431.771
BSS 20	2042	18.81	19.57	18.32	19.79	331.887	-415.190
BSS 21	2428	19.39	20.14	18.88	20.33	528.692	-351.818
BSS 22	2544	19.09	19.78	18.62	20.02	170.663	-335.835
BSS 23	2546	19.36	20.05	18.91	20.23	162.471	-335.651
BSS 24	2547	19.08	19.71	18.65	19.93	152.264	-330.614
BSS 25	2623	18.79	19.49	18.30	19.67	-330.428	-300.632

Table 2—Continued

#	ID	V	B	R	U	X	Y
BSS 26	2749	19.23	19.93	18.76	20.11	-305.596	-305.598
BSS 27	2965	19.25	19.96	18.78	20.10	-293.869	-268.150
BSS 28	2978	18.56	19.19	18.14	19.48	-45.357	-269.560
BSS 29	3171	19.10	19.82	18.61	20.01	193.588	-237.935
BSS 30	3253	18.72	19.30	18.31	19.56	244.559	-231.358
BSS 31	3434	18.60	19.21	18.19	19.46	-799.539	-201.215
BSS 32	3501	18.79	19.47	18.33	19.68	-805.423	-188.600
BSS 33	3568	17.62	18.23	17.21	18.62	166.820	-167.683
BSS 34	3684	18.69	19.49	18.14	19.67	208.239	-157.790
BSS 35	3814	18.60	19.36	18.08	19.57	-59.101	-139.850
BSS 36	4087	19.38	20.15	18.84	20.23	-319.318	-101.848
BSS 37	4157	17.68	18.13	17.36	18.56	-790.025	-91.930
BSS 38	4239	19.39	20.13	18.89	20.29	-492.933	-77.139
BSS 39	4329	19.29	20.07	18.80	20.22	543.722	-30.792
BSS 40	4332	18.32	19.05	17.82	19.23	633.899	-62.242
BSS 41	4337	18.61	19.17	18.22	19.46	739.292	-51.804
BSS 42	4350	19.32	19.97	18.88	20.11	-764.300	-56.442
BSS 43	4431	17.95	18.40	17.61	18.75	186.752	-46.434
BSS 44	4463	18.87	19.49	18.45	19.69	-411.709	-32.642
BSS 45	4469	18.63	19.23	18.22	19.49	295.844	-36.940
BSS 46	4470	19.28	19.90	18.84	20.08	287.043	-32.371
BSS 47	4528	18.87	19.60	18.36	19.82	-70.825	-32.440
BSS 48	4572	19.27	20.05	18.74	20.34	-150.785	-25.653
BSS 49	4723	19.50	20.23	18.97	20.39	-325.664	-1.551
BSS 50	4845	18.58	19.34	18.07	19.75	-82.528	19.827

Table 2—Continued

#	ID	V	B	R	U	X	Y
BSS 51	5111	19.03	19.81	18.49	19.99	-835.504	58.053
BSS 52	5181	18.39	18.99	17.99	19.32	451.931	80.364
BSS 53	5198	18.61	19.34	18.10	19.61	-56.833	69.893
BSS 54	5364	19.28	19.95	18.83	20.20	-198.830	108.252
BSS 55	5514	19.01	19.82	18.47	20.03	-336.323	121.265
BSS 56	5631	18.32	19.00	17.85	19.29	-404.621	146.077
BSS 57	5712	19.13	19.80	18.65	19.97	329.344	150.904
BSS 58	5816	18.52	19.13	18.09	19.43	172.368	179.946
BSS 59	5938	17.85	18.46	17.43	18.90	50.804	191.088
BSS 60	6003	18.04	18.67	17.60	18.89	889.243	202.474
BSS 61	6014	17.58	18.07	17.24	18.50	621.351	212.900
BSS 62	6243	18.32	19.05	17.95	19.42	324.106	250.420
BSS 63	6244	19.08	19.77	18.63	19.95	317.493	259.019
BSS 64	6433	18.91	19.73	18.36	19.97	38.265	280.186
BSS 65	6556	19.19	19.97	18.65	20.11	1065.295	282.922
BSS 66	6594	18.65	19.29	18.21	19.48	-947.905	292.308
BSS 67	6671	18.87	19.54	18.41	19.79	149.435	311.900
BSS 68	6699	18.96	19.77	18.42	19.96	-267.150	322.899
BSS 69	6701	18.99	19.78	18.44	19.99	-282.224	317.300
BSS 70	6797	18.98	19.74	18.52	19.96	114.881	326.295
BSS 71	6817	19.20	19.95	18.67	20.15	472.171	323.492
BSS 72	7298	18.76	19.42	18.31	19.66	-325.091	413.188
BSS 73	7305	18.68	19.30	18.25	19.51	259.097	416.515
BSS 74	7506	18.43	19.16	17.92	19.41	40.085	454.635
BSS 75	7563	19.00	19.74	18.50	19.90	-571.343	465.771

Table 2—Continued

#	ID	V	B	R	U	X	Y
BSS 76	7963	19.08	19.86	18.54	20.01	470.976	541.285
BSS 77	8036	18.04	18.64	17.62	18.87	428.476	568.233
BSS 78	8193	18.19	18.81	17.74	19.07	306.234	601.330
BSS 79	8918	18.20	18.89	17.73	19.10	186.325	809.361
BSS 80	9113	19.04	19.82	18.50	19.99	479.085	879.267
BSS 81	9115	19.23	19.88	18.78	20.07	-528.758	889.671
BSS 82	9294	19.24	20.02	18.71	20.09	288.298	954.655
BSS 83	9297	19.24	19.99	18.73	20.30	564.001	953.698
BSS 84	9317	19.03	19.67	18.58	19.85	-1.994	964.133
BSS 85	9589	19.15	19.87	18.66	20.08	-316.575	-115.017
BSS 86	9599	18.92	19.67	18.47	19.88	17.417	-119.848
BSS 87	9618	18.34	19.05	17.84	19.30	-91.522	-110.438
BSS 88	9688	18.03	18.63	17.60	18.96	11.660	-63.064
BSS 89	9723	19.23	19.92	18.73	20.15	-261.537	-51.061
BSS 90	9740	18.28	19.00	17.80	19.32	-120.423	-35.079
BSS 91	9763	18.31	18.96	17.86	19.23	-18.104	-27.268
BSS 92	9765	19.16	19.92	18.67	20.11	-19.759	-21.688
BSS 93	9797	18.18	18.71	17.83	19.25	-104.733	-15.695
BSS 94	9798	18.59	19.29	18.12	19.59	-115.067	-13.541
BSS 95	9909	18.46	19.10	18.02	19.40	-185.532	66.507
BSS 96	9955	17.59	18.27	17.12	18.61	40.322	84.100
BSS 97	9961	19.13	19.89	18.59	20.13	177.678	71.732
BSS 98	10002	18.69	19.36	18.25	19.65	15.869	106.062
BSS 99	10014	18.31	18.86	17.93	19.22	77.432	115.310
BSS100	10046	18.77	19.57	18.29	19.83	-233.953	123.758

Table 2—Continued

#	ID	V	B	R	U	X	Y
BSS101	10053	19.22	19.92	18.72	20.14	-228.244	132.875
BSS102	10092	17.48	18.12	17.04	18.60	16.717	167.770
BSS103	10159	18.58	19.33	18.13	19.58	108.702	202.048
BSS104	10226	18.40	19.04	18.05	19.05	-194.530	-178.189
BSS105	10277	19.14	19.83	18.66	20.07	-14.713	-80.536
BSS106	10286	19.14	19.87	18.67	20.13	-220.658	-49.144
BSS107	10365	19.02	19.76	18.29	20.04	-46.893	-75.749
BSS108	10376	18.50	19.14	18.04	19.46	75.401	-18.944
E-BSS 1	816	17.31	18.16	16.77	18.46	6.936	-685.088
E-BSS 2	1692	17.33	18.18	16.82	18.60	477.852	-483.990
E-BSS 3	2533	17.14	17.92	16.64	18.39	-142.159	-313.275
E-BSS 4	3437	17.19	17.94	16.68	18.37	768.774	-200.574
E-BSS 5	3442	17.27	18.11	16.75	18.51	-840.575	-188.349

FIGURE CAPTION

Fig. 1 Location of the five FORS1 fields observed in NGC 6712. Four fields were observed at Standard Resolution (SR): Q1,Q2,Q3,Q4 and one at High Resolution (HR), respectively. The HR field is roughly centered on the cluster centre. The cluster centre is located at the origin of the coordinates.

Fig. 2 Calibration curves for the U, B, V, R filters.

Fig. 3 Internal photometric errors for the HR field. The rms values of the frame-to-frame scatter are plotted versus the U, B, V, R magnitude of each star.

Fig. 4 The V, $B-V$ colour magnitude diagramme for the whole sample of stars observed in NGC 6712. In Panel (a) only stars lieing in the FORS-HR field are plotted, while Panel (b),(c) and (d) show stars in annuli at increasing distance from the cluster centre.

Fig. 5 The observed radial density profile for the evolved stellar population (*filled circles*). All stars plotted in Figure 4 with $V < 20$ have been counted. The stellar density has been scaled to match the density profile of unevolved MS stars with $19.5 < R < 20.5$ (corresponding to $\sim 0.75 M_{\odot}$) for $r > 2'$ (*large open squares*) see also Figure 8 in *Paper II*). The dotted horizontal line represents the density of $0.75 M_{\odot}$ star measured in the control field at $42'$ from the cluster centre. The distance $r = 5'$ from the cluster centre is indicated by a vertical arrow.

Fig. 6 The V, $B-V$ colour magnitude diagramme for stars observed in the HR field after the statistical decontamination from field stars (see text)

Fig. 7 HB stars in NGC 6712. The solid heavy line is the V_{ZAHB} level, determined by F99. Seven RR Lyrae variables are plotted as large filled triangles.

Fig. 8 Blue Stragglers Star candidates *(large filled circles)* in NGC 6712. The zoomed CMD in the BSS region in the $(V, B-V)$ *(panel a)* and $(U, U-V)$ *(panel b)*, plane. The 5 objects plotted as *stars* are suspected to be evolved (E-BSS) *i.e.* BSS in the SGB, which have left the MS to evolve toward the RGB.

Fig. 9 Cumulative radial distribution (ϕ) for BSS (heavy solid line) compared to the RGB-SGB (dashed line) as a function of their projected distance (r) from the cluster centre in arcmin.

Fig. 10 $U, U-B$ CMD for NGC 6712 from FORS1-HR images. The bright blue object #9620 is plotted as a *large filled triangle*. The three faint UV stars (plotted as *open triangles*) are discussed in *Paper I*. An isochrone from Bertelli et al. (1994) is also plotted for reference. As can be seen, the bright blue object is located along the post-AGB cooling sequence.

Fig. 11 $(H\alpha, H\alpha - R)$ CMD for NGC 6712 from FORS1-HR images. The $H\alpha$ excess star #10261 (plotted as a *large filled triangle*) is the star discussed in *Paper I*. Blue HB stars (with $B-V<0.5$) are plotted as large filled circles, BSS as selected in Section 6 are plotted as large asterisks. The small open square is the bright blue object discussed in Section 7.1.

Fig. 12 The mean ridge line of NGC 6171 shifted $[\Delta V = 0.62, \Delta(B-V) = 0.0]$ to match the CMD of NGC 6712.

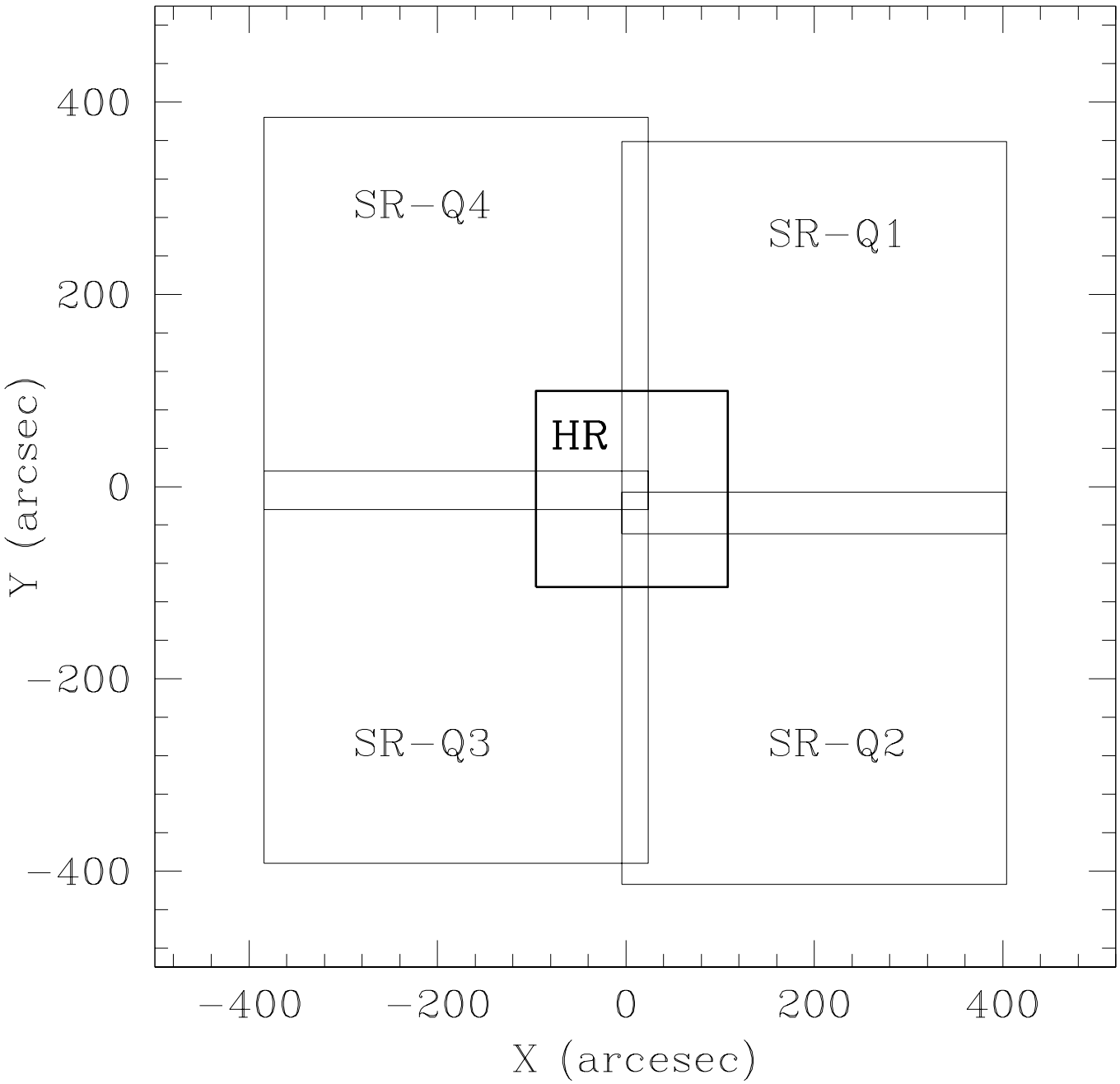
SR−Q4
SR−Q1
HR
SR−Q3
SR−Q2
400
200
0
−200
−400
Y (arcsec)
−400
−200
0
200
400
X (arcesec)

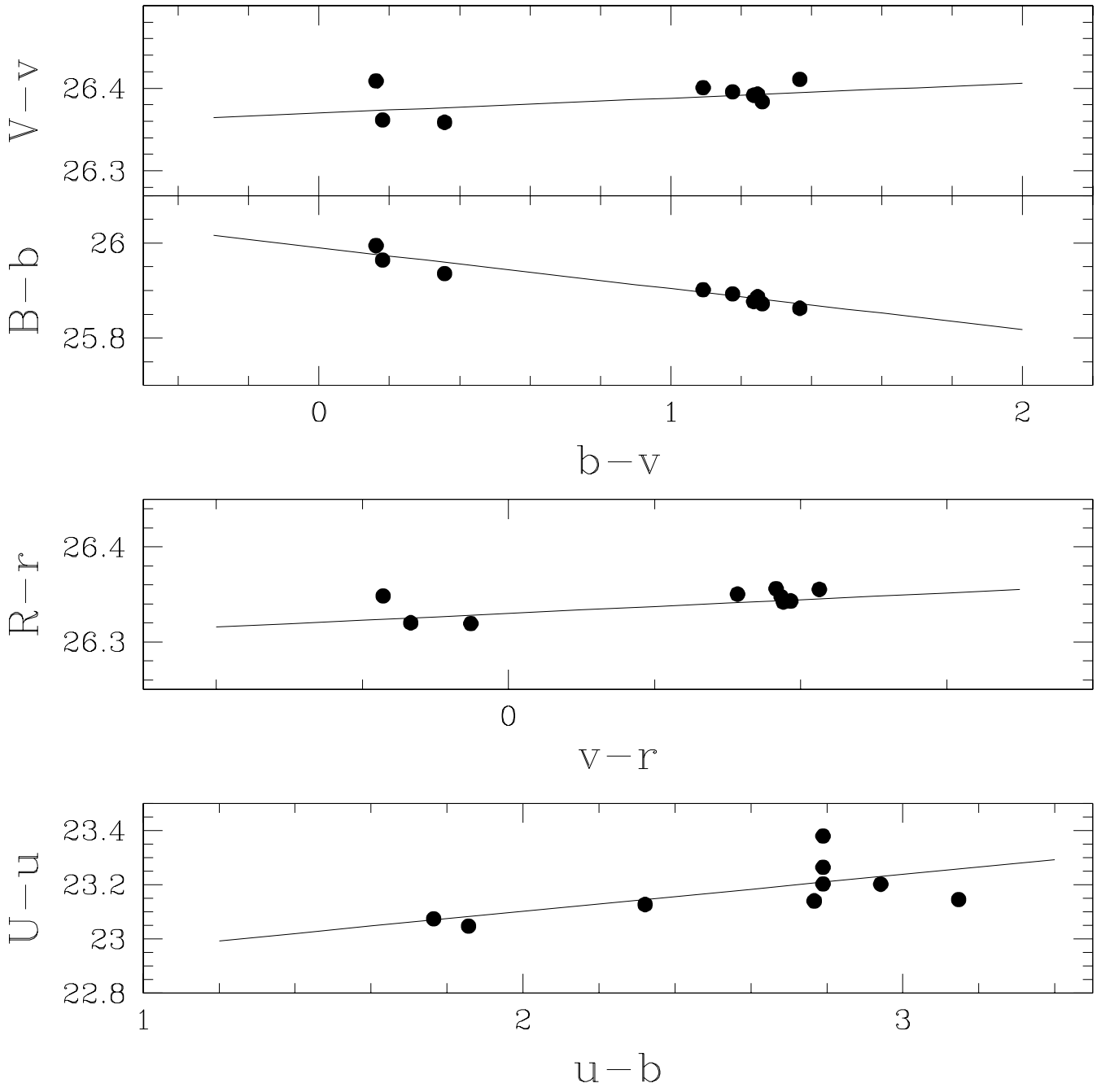
V−v
26.4
26.3
B−b
26
25.8
0
1
2
b−v
R−r
26.4
26.3
0
v−r
U−u
23.4
23.2
23
22.8
1
2
3
u−b

This figure "paltrinieri3.jpg" is available in "jpg" format from:

http://arXiv.org/ps/astro-ph/0102331v1

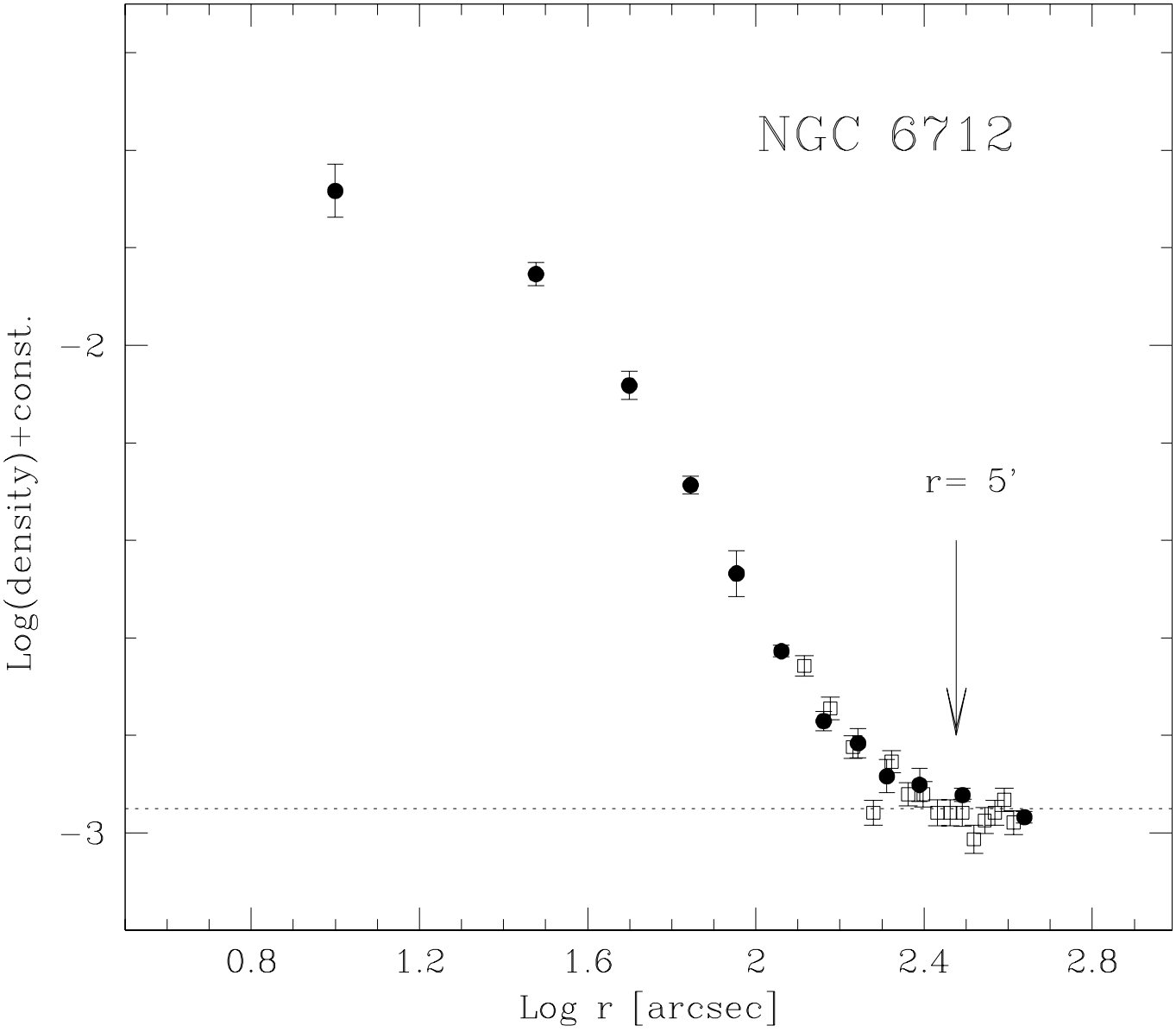
NGC 6712
r= 5'
Log(density)+const.
−2
−3
0.8
1.2
1.6
2
2.4
2.8
Log r [arcsec]

This figure "Paltrinieri6.jpg" is available in "jpg" format from:

http://arXiv.org/ps/astro-ph/0102331v1

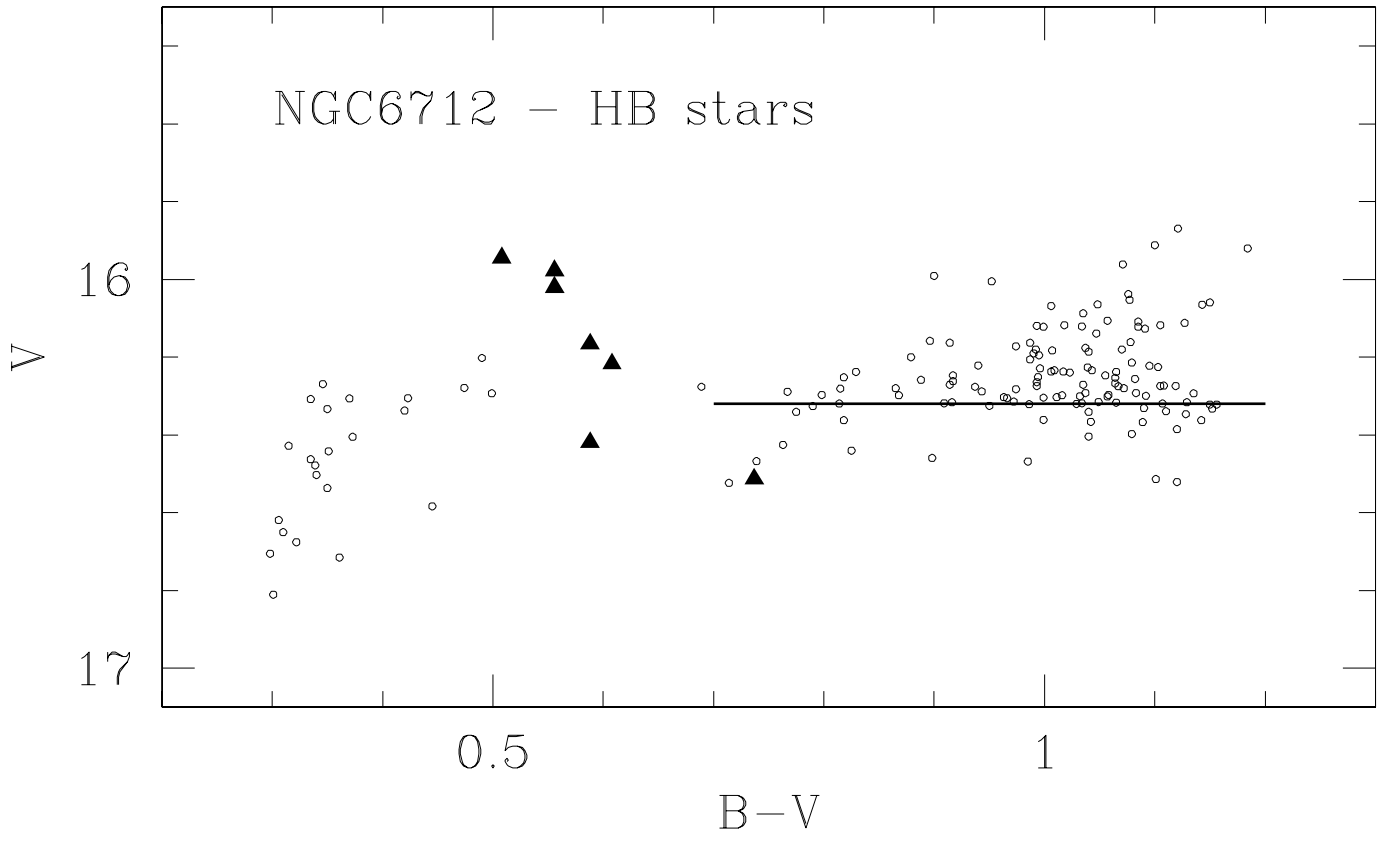
NGC6712 – HB stars
16
17
V
0.5
1
B−V

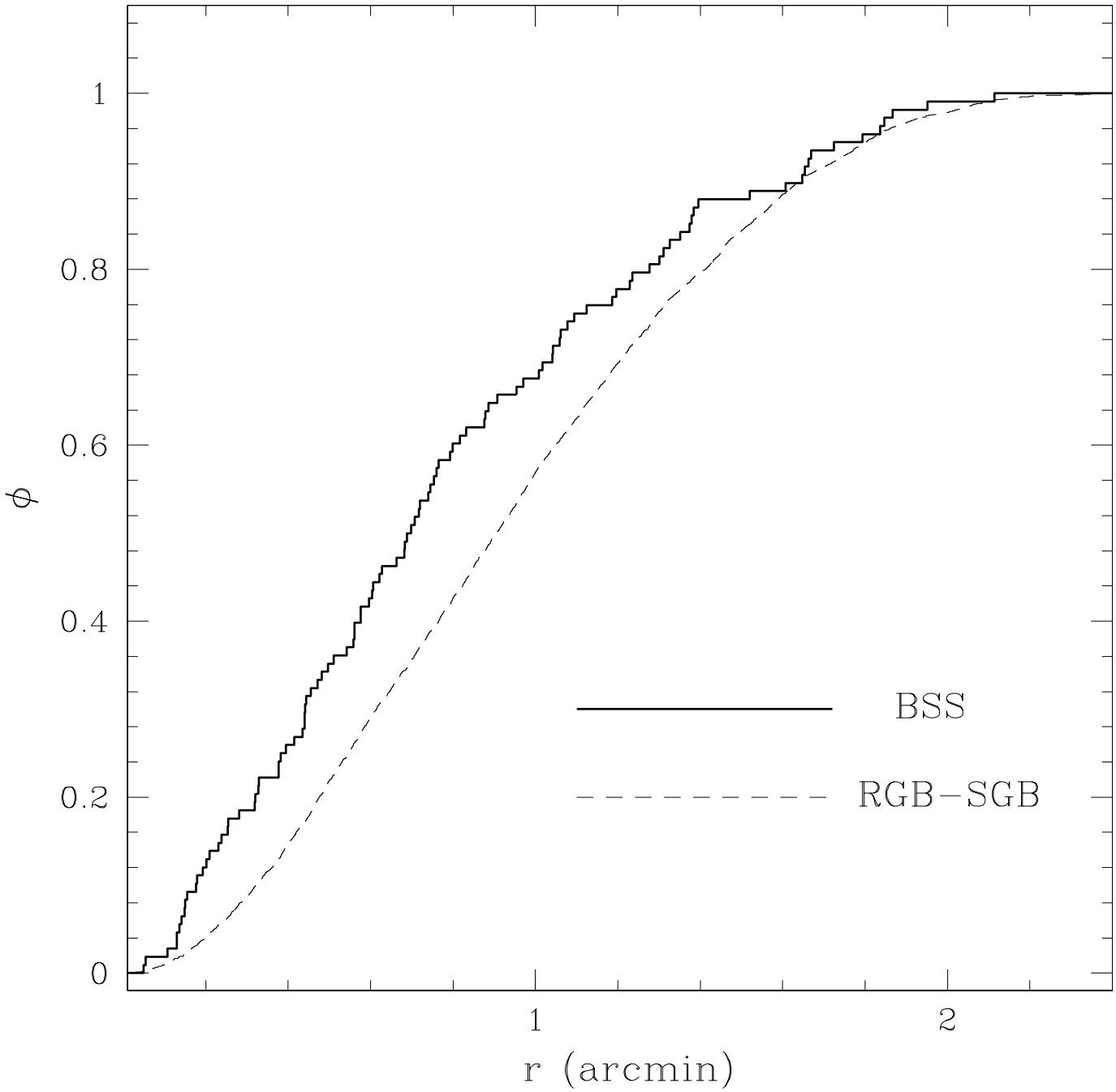
1
0.8
0.6
0.4
0.2
0
ϕ
1
2
r (arcmin)
BSS
RGB−SGB

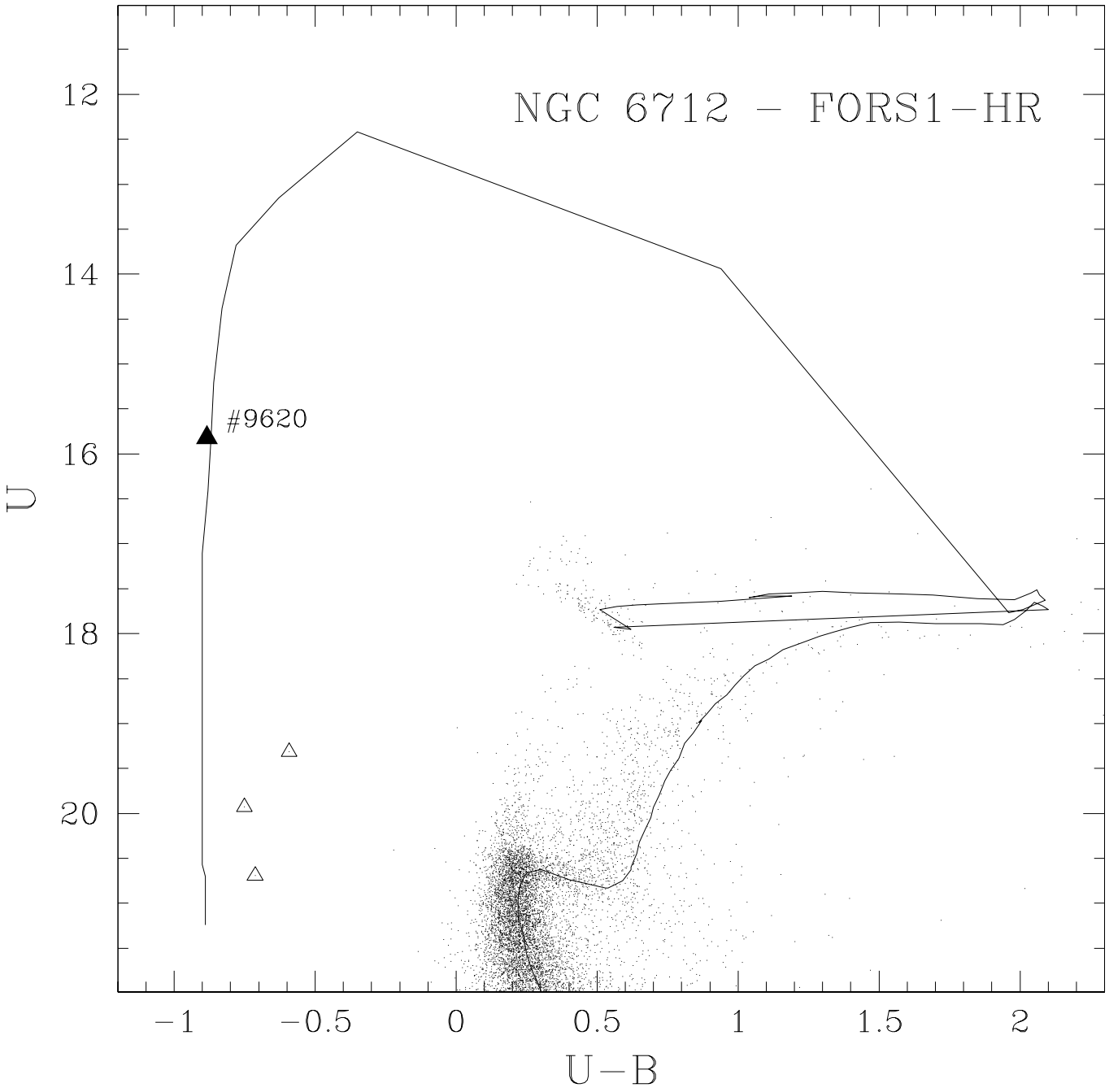
NGC 6712 – FORS1–HR
#9620
U
U–B
12
14
16
18
20
−1
−0.5
0
0.5
1
1.5
2

This figure "paltrinieri11.jpg" is available in "jpg" format from:

http://arXiv.org/ps/astro-ph/0102331v1

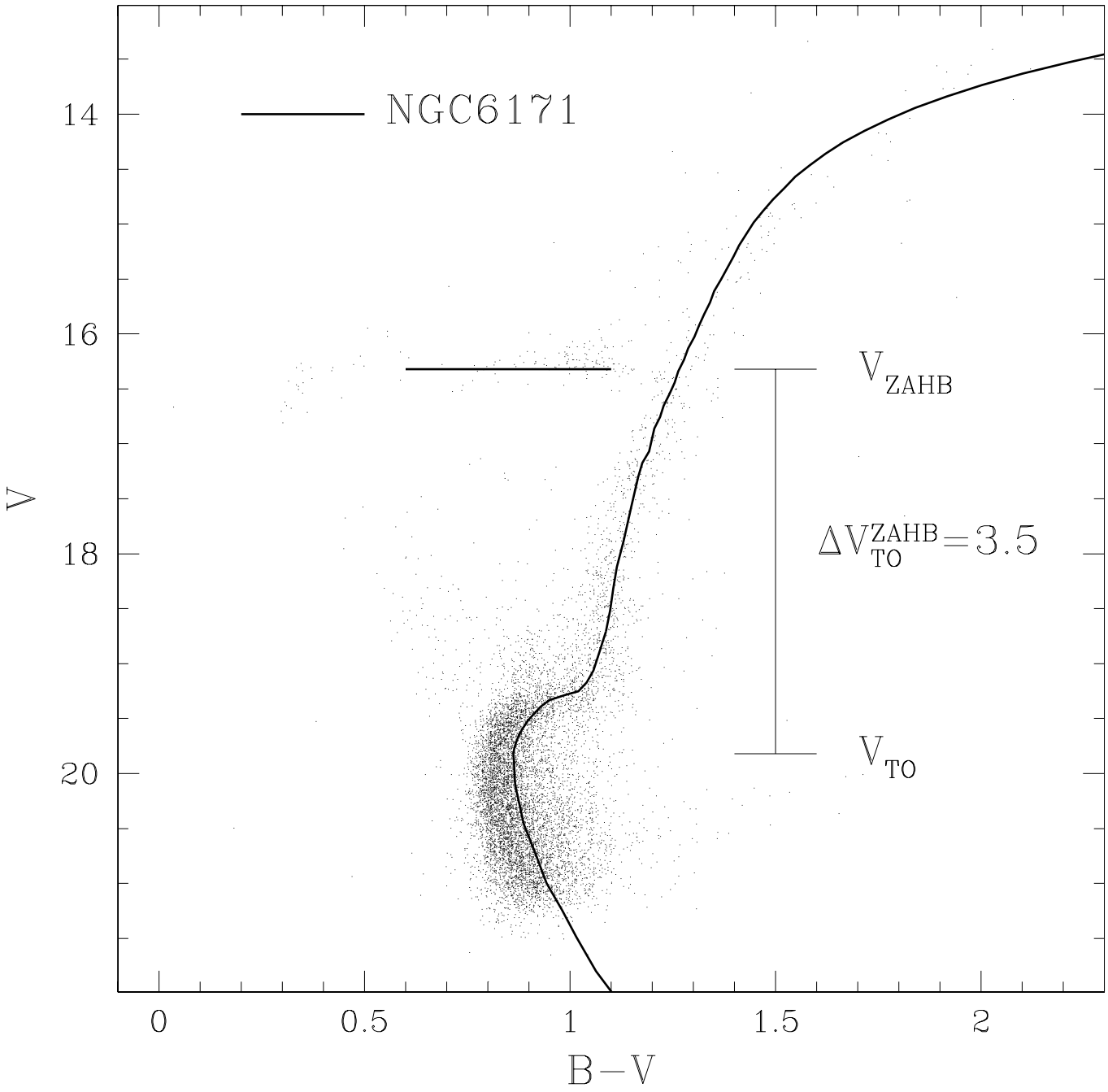
NGC6171
14
16
18
20
V
0
0.5
1
1.5
2
B−V
V_{ZAHB}
$\Delta V_{TO}^{ZAHB}=3.5$
V_{TO}